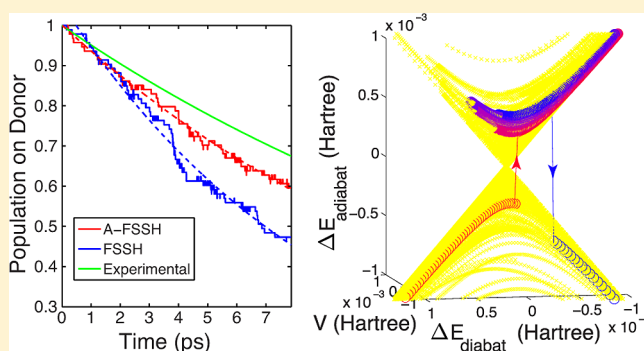


# Quantifying the Lifetime of Triplet Energy Transfer Processes in Organic Chromophores: A Case Study of 4-(2-Naphthylmethyl)benzaldehyde

Brian R. Landry\* and Joseph E. Subotnik

Department of Chemistry, University of Pennsylvania, 231 S. 34th Street, Philadelphia, Pennsylvania 19104, United States

**ABSTRACT:** We simulate the dynamics of triplet–triplet energy transfer in a donor–bridge–acceptor system [4-(2-naphthylmethyl)benzaldehyde] with surface hopping, using electronic energies, gradients, and derivative couplings that are calculated on the fly. Using Boys localization to diabaticize electronic states, we calculate energy transfer rates that agree favorably with experiment. The atomistic nature of our dynamical investigation produces several unique insights into this energy transfer reaction including an approximation of the decoherence time for the energy transfer process and the observation that the reaction pathway passes through a conical intersection.



## 1. INTRODUCTION

Twenty-five years ago, Closs and co-workers carried out pioneering work into electronic energy transfer in a donor–bridge–acceptor system (donor = 4-benzophenonyl, acceptor = naphthyl).<sup>1,2</sup> Their photolysis experiments investigated triplet–triplet energy transfer with the goal of highlighting the quantitative similarities between electronic energy transfer (EET) and electron transfer (ET). They demonstrated that triplet–triplet energy transfer, like electron transfer, exhibited an exponential scaling with bridge length in agreement with the exchanged-based Dexter mechanism. Furthermore, they showed that, to a reasonable approximation, the rate of electronic energy transfer is proportional to the product of the rate of electron transfer and the rate of hole transfer. In combination, these results strengthened the idea that electron transfer and electronic energy transfer should be thought of as two examples of the same nonadiabatic process. To that end, recent theoretical and computational work has taken advantage of this parallelism to calculate energy transfer rates via the celebrated Marcus formula<sup>3</sup> for electron transfer rates.<sup>4,5</sup> A key breakthrough in the field of electronic structure has been the realization that diabatic states can be calculated for EET just as for ET; one can use a localized diabaticization scheme to determine the parameters that enter into the Marcus rate equation.<sup>6–12</sup>

Unfortunately, Marcus theory is limited by the applicability of two approximations: the harmonic assumption and the Condon approximation. While the harmonic approximation for free energy surfaces has been shown to be valid in many cases,<sup>13</sup> the Condon approximation has no such broad applicability. In particular, the Condon approximation stipulates that the diabatic coupling (i.e., the Hamiltonian matrix element between the state with the excitation localized on the donor and the

state with the excitation localized on the acceptor) must be constant throughout the energy transfer process.<sup>14</sup> In practice, for intramolecular donor–bridge–acceptor systems, the Condon approximation holds only when rigid bridges hold the orbitals of the donor and acceptor molecular fragments close to a fixed configuration and thus preserve a constant diabatic coupling. Given this limitation, many authors have attempted to go beyond Marcus theory and calculate ET and EET rates including non-Condon effects but still in the context of a Fermi golden rule transition state theory.<sup>15,16</sup>

In this paper, we will go beyond Marcus theory (and transition state theory in general) to study a Closs-type system with a flexible bridge. Our focus is on compound M, 4-(2-naphthylmethyl)benzaldehyde,<sup>17</sup> shown in Figure 1, where the bridge is a simple methylene unit. Unlike the case for larger

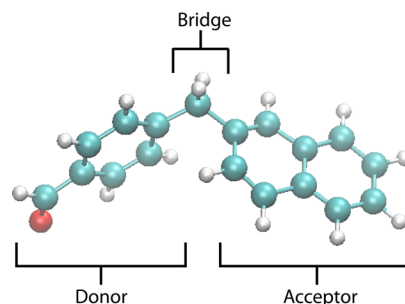


**Figure 1.** Molecule under investigation: 4-(2-naphthylmethyl)-benzaldehyde, Closs compound M. The donor is 4-benzaldehydyl, the bridge is methylene, and the acceptor is naphthyl.

Received: July 8, 2014

Published: September 24, 2014

rigid molecules (with parabolic energy surfaces and constant diabatic coupling), the EET process for compound M cannot naively be explained by Marcus theory.<sup>3</sup> In particular, because the flexible methylene bridge on compound M allows the orientation of the donor and acceptor ring systems to fluctuate significantly and because the diabatic coupling depends sensitively on the overlap of the pi-systems on each ring, the diabatic coupling is not constant. For instance, Figure 2 shows

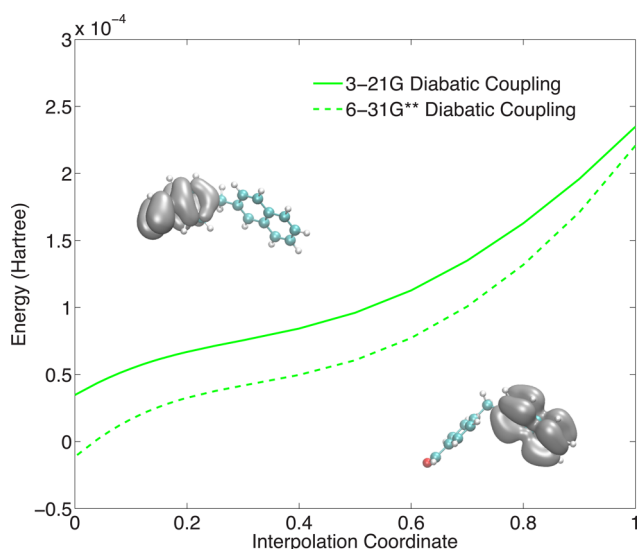


**Figure 2.** Plot of the CIS diabatic coupling for compound M at different geometries interpolated between the optimized geometry for the excitation on the donor and the optimized geometry for the excitation on the acceptor. Two basis sets are used here: 3-21G and 6-31G\*\*. The optimizations were done in the 6-31G\*\* basis set. The plot shows that the 3-21G couplings (which were used for our simulations) are rather similar to those calculated using a larger basis set (6-31G\*\*). On the left, we show the excitonic particle localized on the donor; on the right, the excitonic particle on the acceptor.

that over the course of an interpolation between the donor-excited and the acceptor-excited geometries, the diabatic coupling changes by an order of magnitude. Thus, it is unclear how to apply Marcus theory. At what geometry do we evaluate the diabatic coupling? At the transition state? At the optimized donor geometry? Clearly, the Condon approximation is violated for this system. Figure 3 also shows that the potential energy surfaces of compound M are extremely anharmonic around the coupling region. For this reason, there is no simple mapping of molecular motions in compound M onto the harmonic Hamiltonian required by Marcus theory, although approximations would be possible if one could find harmonic free energy curves for some abstract reaction coordinate.

In the end, we would like to calculate the EET rate for compound M in a stable fashion and gain insight into the coupled nuclear–electronic dynamics of this EET process without relying on the assumptions of Marcus theory. To do so, we utilize surface hopping dynamics<sup>18</sup> with two different flavors: standard fewest switches surface hopping (FSSH) without decoherence and our augmented FSSH (A-FSSH) that incorporates decoherence.<sup>19</sup> Combined with *ab initio* on-the-fly electronic structure (energies, gradients, and derivative couplings), we can calculate the total rate of EET and compute the decoherence time for individual EET events (for details, see Section 3).

In recent years, several research groups have studied EET for real (i.e., not model) systems using atomistic simulations and various approaches. Aspuru-Guzik and co-workers investigated EET using molecular dynamics force fields while approximating that the dynamics were effectively on the ground state without full quantum feedback.<sup>20</sup> Rhee and co-workers have used the Poisson bracket mapping equation<sup>21</sup> to simulate some quantum feedback while using a semiempirical Hamiltonian to describe the exciton.<sup>22</sup> Rossky and Tretiak have explored EET extensively using a combination of semiempirical force fields and FSSH.<sup>23,24</sup> These authors have also studied decoherence time scales with some popular schemes from the literature.<sup>25</sup> With regard to real time *ab initio* nonadiabatic dynamics in general (i.e., not EET), over the last 15 years, Martinez has studied many cases of nonadiabatic electronic relaxation using a combination of multiple spawning and active space electronic structure.<sup>26</sup> Many others have studied electronic relaxation using FSSH and active space electronic structure theory<sup>27</sup> or TD-DFT.<sup>28</sup> Keeping this long history in mind, we believe this manuscript is the first atomistic simulation of electronic energy transfer for a donor–bridge–acceptor system using blackbox *ab initio* potential energy surfaces (i.e., without resorting to a semiempirical description) and the first attempt to quantify a decoherence time for an EET process using such a simulation with *ab initio* electronic structure.

We organize this paper as follows: Section 2 provides an overview of the triplet–triplet energy transfer in the Closs system. Section 3 discusses our methods. Section 4 gives the results of our simulations, and Section 5 discusses their consequences. Finally, we conclude in Section 6.

## 2. TRIPLET–TRIPLET ELECTRONIC ENERGY TRANSFER IN THE CLOSS SYSTEM

Pump–probe experiments<sup>1</sup> reveal that three excited electronic states are involved in energy transfer in the Closs systems: the first excited singlet state and the first two triplet states. After the ground state is photoexcited to the first singlet state, the molecule undergoes a fast intersystem crossing to the first excited triplet state mediated by spin–orbit coupling. This first triplet state can be visualized as two wells (Figure 3) with each well representing a different localization of the excitation. For one well, the excitation is localized on the donor molecule, and for the other well, the excitation is localized on the acceptor molecule. After the intersystem crossing to the triplet state, the system finds itself in the donor well. Henceforth, the dynamics proceed almost entirely on the first triplet state with the exception of possible transitions to the second excited state at the crossing region; the  $T_1/T_2$  crossing region is near the transition state between the donor and acceptor wells. After relaxation into the acceptor well, the system undergoes a much slower relaxation back to the ground state (either via phosphorescence or radiationless decay). The simulation in this paper will focus on the  $T_1/T_2$  triplet energy transfer and will ignore the longer relaxation to the ground state.

For our purposes, it is useful to think about the triplet electronic states in two ways. First, from the adiabatic perspective, the  $T_1$  and  $T_2$  electronic states are the mathematical solutions to the electronic Schrödinger equation. Second, from a diabatic perspective, a unitary transformation of the adiabatic states can yield meaningful donor and acceptor states (Figure 3). For calculating EET rates, diabatic state populations on the donor and acceptor are the relevant quantities.

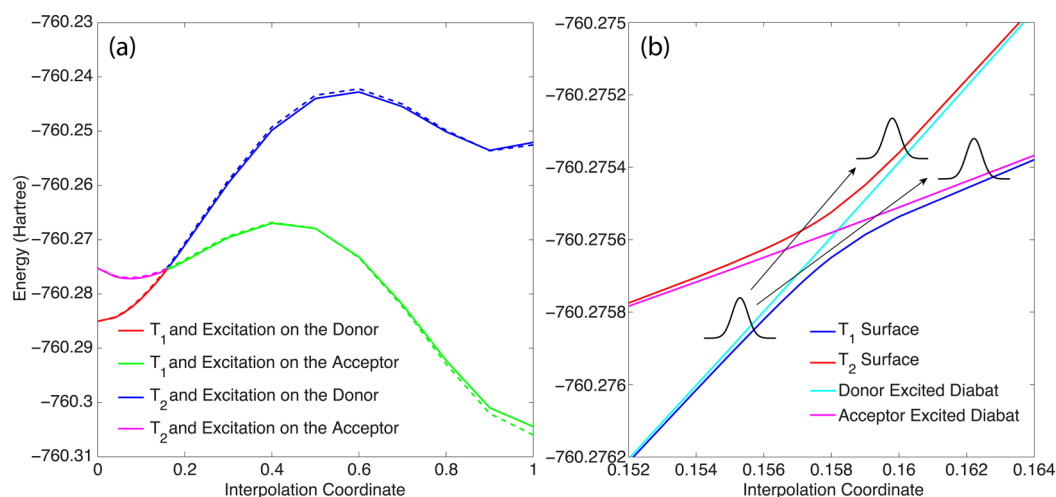


**Figure 3.** Plot of the states involved with the triplet–triplet electronic energy transfer at different geometries interpolated between the optimized geometry for the excitation on the donor and the optimized geometry for the excitation on the acceptor (the optimizations were done in the 6-31G\*\* basis set). (a) The surfaces can be visualized as the upper and lower adiabatic surfaces ( $T_2$  and  $T_1$ ) or left and right diabatic surfaces (excitation found on the donor and excitation found on the acceptor). The coloring scheme highlights these two ways to view the electronic states. In the adiabatic basis, the  $T_1$  state is given by the red and green surfaces, and the  $T_2$  state is given by the magenta and blue surfaces. In the diabatic basis, the donor state is given by the red and blue surfaces, and the acceptor state is given by the magenta and green surfaces. (See section 2 for further discussion.) The states were calculated using CIS with two different bases: 3-21G (solid) and 6-31G\*\* (dotted). The 6-31G\*\* surfaces were shifted by a constant energy so that the lower surfaces agreed at interpolation coordinate 0. (b) A detail of the coupling region showing how the diabatic states cross and form beginning and ending states for EET, while the adiabatic states obey the noncrossing rule. Decoherence rates correspond to the time needed for wavepackets on the donor and acceptor diabats to separate.

### 3. METHODS

#### 3.1. Tully-Style Fewest Switches Surface Hopping.

Surface hopping was our choice of dynamics method to simulate the electronic and nuclear dynamics. The central idea behind surface hopping dynamics is to represent a quantum nuclear wavepacket as a swarm of independent classical nuclear trajectories.<sup>18</sup> Outside of coupling regions, a quantum wavepacket moves along a single adiabatic potential energy surface. In keeping with this physical reality, each independent classical surface hopping trajectory also moves along a single active electronic potential energy surface, responding to the force of that surface only. Along with nuclear positions and momenta, each trajectory also carries an electronic wave function that keeps track of the probability of measuring the electrons in each adiabatic state, and the electronic wave function is propagated forward in time by the time-dependent Schrödinger equation with the nuclear positions as parameters. To model non-adiabatic transitions, a trajectory has some probability to hop from one adiabatic surface to another during each time step. According to Tully, the probability of hopping depends on the probability of measuring the electron on the new surface as well as the momentum and derivative coupling.<sup>18</sup> It is given by

$$\gamma_{ij}^{\text{hop}} = 2dt \text{Re}(c_i^* \vec{c}_j \cdot \vec{R} \cdot \vec{d}_{ij}) / |c_i|^2 \quad (1)$$

where  $dt$  is the time step,  $c_i$  is the  $i$ th component of the electronic wave function,  $\vec{R}$  is the nuclear velocity, and  $\vec{d}_{ij}$  is the derivative coupling between the  $i$ th and  $j$ th electronic states.

**3.2. Trajectory Details.** To initialize the energy transfer dynamics for Closs compound M (Figure 1) using FSSH, we required a thermalized distribution on the  $T_1$  state in the donor excited basin. To generate such a distribution, we ran trajectories starting from the ground state nuclear geometry of the donor well for 5000 au (about 121 fs) entirely on the first triplet state and with a Langevin thermostat at 300 K. We

used this thermalized distribution of positions and momenta for our subsequent dynamical simulation of the electronic energy transfer. Note that in thermalizing along  $T_1$ , we assume that the intersystem crossing rate is faster than the triplet–triplet transfer rate,  $k_{\text{ISC}} > k_{\text{TT}}$ .

For the surface hopping dynamics<sup>18,19</sup> (see Section 3.1 for a description of the method), electronic structure calculations were carried out on the fly. As required for the surface hopping algorithm, energies, gradients, and derivative couplings were all computed at each time step with the QChem package configuration interaction singles (CIS) using a 3-21G basis set.<sup>29,30</sup> Admittedly, 3-21G is a small basis set, and our results should not necessarily be expected to have quantitative accuracy. Our choice of basis set and method was justified on the following grounds:

(1) CIS has been used to successfully reproduce transition rates for rigid donor–bridge–acceptor molecules using Marcus theory.<sup>5</sup>

(2) The 3-21G and 6-31G\*\* diabatic couplings are similar (Figure 2), and the diabatic state energies are also very similar (Figure 3). Admittedly, the reorganization energies are a bit different in 3-21G and 6-31G\*\* (Section 5).

The nuclear dynamical equations were integrated using a variable time step of either 30 or 0.5 au (0.726 or 0.0121 fs) depending on the probability of hopping.<sup>31</sup> The time step for propagating the electronic equations of motion was always 0.5 au units (0.0121 fs), and the nuclear coordinates and momenta at each time point were determined by interpolation for intervals when the nuclear equations were being integrated using the longer time step. Because the electronic structure calculations were the computational time bottleneck, using these timesteps allowed for a slower more accurate integration of the surface hopping equations within the coupling regions and for faster integration outside the coupling regions. Tretiak

and co-workers have written extensively of the necessary tricks needed to run FSSH calculations efficiently.<sup>32</sup>

To calculate averages, we ran 96 independent trajectories for 20,000 timesteps (up to 15 ps). Surface hopping dynamics were carried out for two triplet electronic states ( $T_1/T_2$ ). Intruder states did appear (but only away from the coupling region); for about 20% of trajectory time, crossings between higher electronic states ( $T_2/T_3$ ) occurred, interfering with a two state diabaticization. Individual trajectories required up to 51 days of computer wall time. For each trajectory, we recorded the nuclear positions and momenta, electronic wave function, active adiabatic electronic surface, and CIS dipole matrices.

**3.3. Diabatization and Diabatic Populations.** Using the matrices and vectors described above, we were able to calculate diabatic states with BoysOV localization for each trajectory on the fly.<sup>5</sup> According to BoysOV diabaticization, diabatic states are constructed by maximizing the distance between the excitonic attachment densities and the distance between excitonic detachment densities. In other words, the function that is maximized is

$$f_{\text{BoysOV}}(\{\Xi_i\}) = \sum_{i,j=1}^{N_{\text{states}}} |\langle \Xi_i | \vec{\mu}^{\text{occ}} | \Xi_i \rangle - \langle \Xi_j | \vec{\mu}^{\text{occ}} | \Xi_j \rangle|^2 + |\langle \Xi_i | \vec{\mu}^{\text{virt}} | \Xi_i \rangle - \langle \Xi_j | \vec{\mu}^{\text{virt}} | \Xi_j \rangle|^2 \quad (2)$$

where  $\vec{\mu}^{\text{occ}}$  and  $\vec{\mu}^{\text{virt}}$  are the dipole operator for the occupied and virtual orbitals, respectively, and the set of states,  $\{\Xi_i\}$ , represents the diabatic states, which are formed via a unitary transformation from the adiabatic states. Our group has recently shown that this formalism yields derivative couplings that are negligible in size.<sup>33,34</sup>

As far as calculating diabatic populations, we determined the diabatic populations as a function of time by averaging the active diabats over all trajectories for each time step. More sophisticated approaches (i.e., those discussed in ref 35) produced the same result because the diabatic coupling was small enough to match up adiabats and diabats at most points in configuration space.<sup>36</sup> This simple adiabatic–diabatic correspondence for each trajectory makes more sophisticated approaches to determining the diabatic state unnecessary. To assign the “active diabatic” state, we simply compared diabatic dipole moments with donor/acceptor centers of mass.

**3.4. The Decoherence Problem and Augmented Fewest Switches Surface Hopping.** One of the known issues of standard fewest switches surface hopping (FSSH) is that its asymmetrical treatment of the nuclear (classical) and electronic (quantum) degrees of freedom leads to an overcoherent electronic wave function. In particular, FSSH does not allow for nuclear wavepackets on different electronic surfaces to fully separate such that the electronic coherence is fully destroyed. There is much literature on this overcoherence of the electronic wave function in FSSH, and this section will only give a short summary of the problem, with a brief discussion of our approach to adding decoherence to FSSH (for complete references, see refs 37–53). One way to understand the decoherence problem is to consider the exact quantum dynamics of a simple nonadiabatic transition. If a fully quantum nuclear wavepacket goes through a nonadiabatic crossing region, the result will be a superposition of two wavepackets on the other side. As the wavepackets separate, the coherence between the two electronic states decreases. However, this loss of coherence is not taken into account by

the standard FSSH method because the electronic wave function,  $\tilde{\psi}$ , is not adjusted appropriately.

Another way to understand the decoherence issue uses the special role of measurement in the classical quantum correspondence. From this perspective, the classical nuclear positions correspond to an effective measurement of the nuclear position at each time step. As a result, when the electronic states lose coherence, it is not possible to get that coherence back, and we must collapse the electronic wave function onto the surface that the trajectory is moving along. From this quantum–classical point of view, decoherence is a fairly straightforward phenomenon because recoherence is impossible.

To address the decoherence problem, we implemented A-FSSH, our version of surface hopping that takes decoherence into account. A-FSSH adds stochastic decoherence events based on a model of separating wavepackets with no additional parameters.<sup>19</sup> In A-FSSH, we keep track of additional dynamical variables: position and momentum moments. Relative to the active adiabatic surface, these moments give the effective position in phase space of a nuclear wavepacket on the other adiabatic surfaces. Using this information, we can calculate an effective decoherence probability for each trajectory, which we use to make stochastic collapsing events (see ref 19 for details).

## 4. RESULTS

### 4.1. Diabatic Populations and Calculated Energy Transfer Rate.

In Figure 4, we plot the populations on the

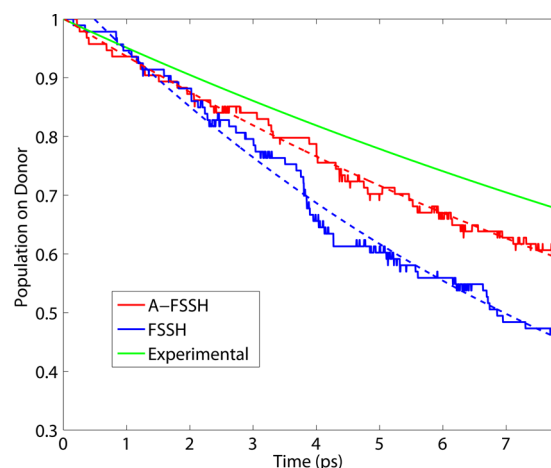


**Figure 4.** Plot of diabatic population as a function of time for the Closs system comparing A-FSSH and FSSH with an exponential based on the experimental decay rate. The dashed lines are exponential fits that give decay times of 15 ps for A-FSSH and 9.3 ps for FSSH. The experimental decay time is 20 ps.<sup>1,54</sup>

donor diabats as a function of time for FSSH (which ignores decoherence) and A-FSSH (which incorporates decoherence). Energy transfer rates are obtained by fitting an exponential to these diabatic populations. Both rates are within a factor of 2 of the experimental rate. Although A-FSSH and FSSH do not give drastically different results, the A-FSSH rate is closer to the experimental rate. As a general rule, adding a decoherence corrections on top of surface hopping trajectories slows down nonadiabatic transfer rates. Given the similarity of the A-FSSH and FSSH transition rates, *if the Condon approximation were to hold*, our previous work studying FSSH and A-FSSH in the



spin-boson model would allow us to put this result in perspective.<sup>55</sup> In that study, for a spin-boson system, we showed that the two methods yield similar rates when the diabatic coupling is large enough such that the system undergoes only a handful of crossing events before relaxation, but small enough so that Marcus theory applies.<sup>56</sup> Therefore, the comparability between the A-FSSH and FSSH rates suggests that because of the short methylene bridge, if the diabatic coupling were indeed constant, compound M would not be very far into the nonadiabatic Marcus regime. From this conclusion, one might further wonder if there could be experimental signatures of coherent EET for compound M.

**4.2. Electronic Decoherence Rate.** Given the wide interest in coherent EET,<sup>57,58</sup> we sought to quantify a decoherence time for the EET process in compound M. To that end, we recorded the time difference between a hop (both accepted and forbidden) and a collapse event, plotting the results in a histogram (Figure 5). We then fit an exponential

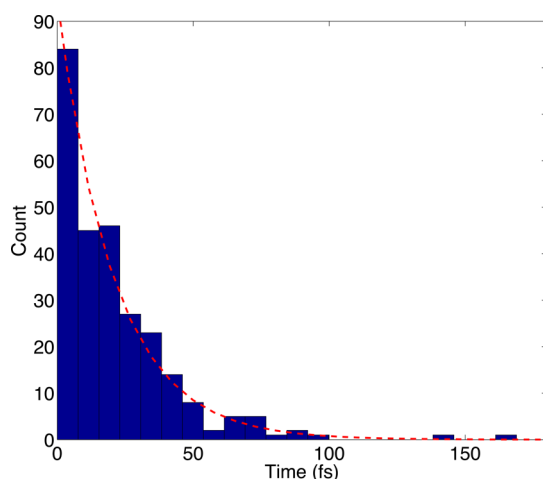


**Figure 5.** Histogram of decoherence times for all A-FSSH trajectories. The time between a hop (either accepted or forbidden) and a decoherence event was recorded for each hop. There were a total of 267 hopping (or attempted hopping) events that led to 266 decoherence events; all data points were distributed among 100 bins (one decoherence event was at a time longer than the range of this plot). The exponential fit shows a decay time of about 20 fs.

curve to the histogram data in order to get a decoherence rate.<sup>59</sup> Even though the dynamics of compound M are simulated in the gas phase, we do not expect that nonpolar solvents will greatly affect the decoherence time (the solvent in ref 1 was benzene).

According to Figure 5, we find a decoherence time of only 20 fs. This decoherence time is extremely fast, a factor of only two more than the period of oscillation of a hydrogen molecule (this extremely fast time scale is consistent with the decoherence time of a few femtoseconds for a hydrated electron as calculated by Rossky and coworkers<sup>39</sup>). This suggests that the crossing region, where the system can be in a superposition of  $T_1$  and  $T_2$  states, is very sharp. Our observations from individual trajectories agrees with this hypothesis; the molecule typically stays in the intersection region for only a few femtoseconds. Once the molecule leaves the crossing region, the different forces on the two surfaces lead quickly to the separation of nuclear wavepackets on the different surfaces and therefore a loss of coherence. This recognition of an extremely fast crossing event led us to search

for a good reaction coordinate and to investigate the topology of the intersection region.

**4.3. Diabatization and an Effective Reaction Coordinate.** A useful reaction coordinate picture of the energy transfer reaction can be constructed according to BoysOV localized diabaticization (Section 3.3).<sup>5,12</sup> Figure 6 shows the

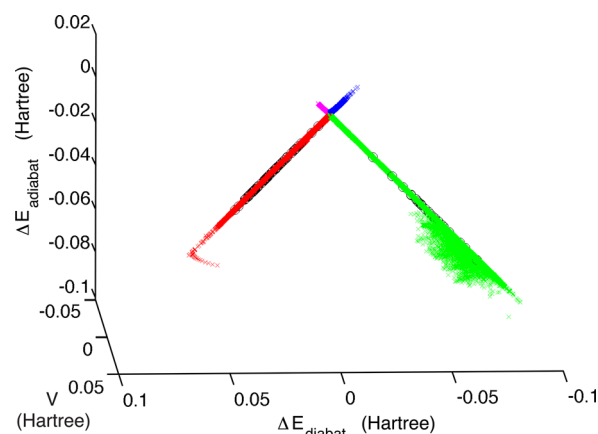


**Figure 6.** Scatter plot for all A-FSSH trajectory points of the difference between adiabatic energies ( $\Delta E_{\text{adiabat}}$ ) as a function of the difference between diabatic energies ( $\Delta E_{\text{diabat}}$ ) and the diabatic coupling ( $V$ ); note that  $\Delta E_{\text{adiabat}}^2 = \Delta E_{\text{diabat}}^2 + 4V^2$ . The difference in diabatic energies and diabatic coupling form an effective reaction coordinate for the energy transfer process. Colors have the same significance as in Figure 3. Black circles represent time steps that had a decoherence event.

result of plotting the difference in adiabatic energies ( $\Delta E_{\text{adiabat}}$ ) as a function of the difference in diabatic energies ( $\Delta E_{\text{diabat}}$ ) and the diabatic coupling ( $V$ ); note that  $\Delta E_{\text{adiabat}}^2 = \Delta E_{\text{diabat}}^2 + 4V^2$ . This figure allows a clear picture for interpreting trajectories that start in the diabatic well of the donor and end in the diabatic well of the acceptor after going through the crossing region. In particular, just as for standard Marcus theory, the diabatic energy difference is a useful reaction coordinate.<sup>14</sup> Furthermore, the set of coordinates ( $V, \Delta E_{\text{diabat}}, \Delta E_{\text{adiabat}}$ ) is the natural framework to observe a conical intersection. The point (0,0,0) represents a diabatic coupling of zero, a difference in diabatic energies of zero, and degenerate adiabatic surfaces from which a conical intersection may branch out.

Combined with trajectory information, the difference in diabatic energies and diabatic coupling serve as effective reaction coordinates that allow us to understand the progress of the reaction. Trajectories start in the donor well and explore reaction space in that region. Eventually, trajectories head toward the crossing region, where they can either (i) hop and end up on the upper adiabatic surface  $T_2$  or (ii) not hop and continue into the acceptor well (Figure 7). The trajectories that do hop return to the crossing region where the great majority of these trajectories hop down and head back to the donor well (Figure 8). A few trajectories do not hop down after returning to the crossing region and continue to explore the nuclear space on  $T_2$  in a more complicated way (Figure 9). Once a trajectory reaches the acceptor well, the extra energy is spread over the many nuclear degrees of freedom, and the trajectory never climbs back into the crossing region.

The effective reaction coordinates in Figure 6 also provide a framework for understanding decoherence. The black circles plotted in Figure 6 represent points at which the trajectory

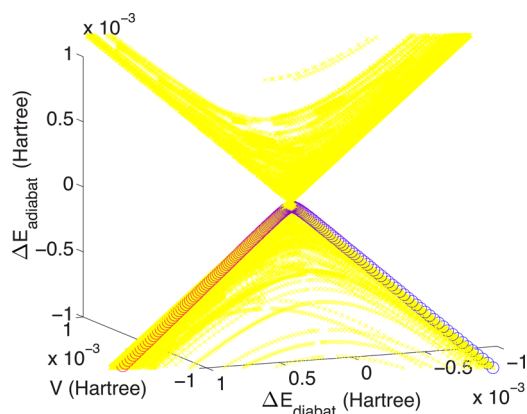


**Figure 7.** Detail of the crossing region showing a single trajectory that relaxes straight from the donor into the acceptor well without hopping. The color change from red to blue illustrates increasing time. The yellow background represents a scatter plot of all other trajectory points in our simulation.

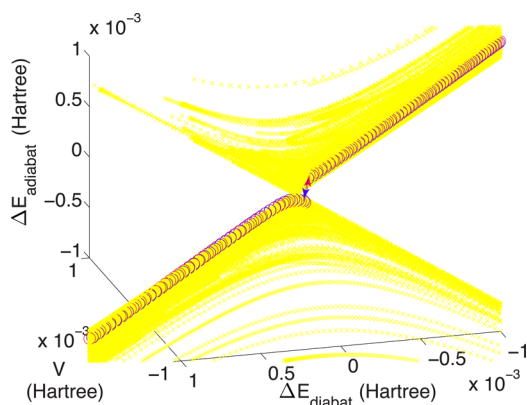


**Figure 8.** Detail of the crossing region showing a single trajectory that hops onto the  $T_2$  adiabatic surface before hopping back down onto the  $T_1$  adiabatic surface and continuing back into the donor well (which is of course on the  $T_1$  surface). The color change from red to blue illustrates increasing time. The yellow background represents a scatter plot of all other trajectory points in our simulation.

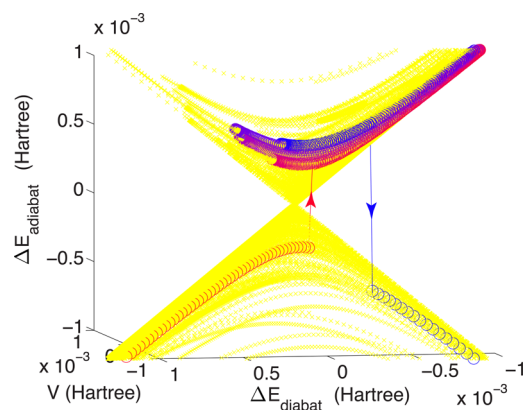


**Figure 9.** Detail of the crossing region showing a single trajectory that jumps to the excited adiabatic surface and explores the  $T_2$  adiabatic surface for some time before hopping down onto the  $T_1$  adiabatic surface and relaxing into the acceptor well (which is of course on the  $T_1$  surface). The color change from red to blue illustrates increasing time. The yellow background represents a scatter plot of all other trajectory points in our simulation.

underwent a decoherence event. The important feature to note from this plot of collapsing events is that none of the decoherence events happen right in the coupling region. In the coupling region, it is possible for superpositions of the two electronic states to persist, and the amplitude of each state in this superposition is important for determining which electronic state will be active once the surface hopping trajectory emerges from the coupling region. As a result, decoherence events should not and do not (according to A-FSSH) occur within the coupling region. Once outside of the coupling region, however, the differing forces on the two surfaces cause the nuclear wavepackets to separate, and decoherence should and does occur naturally.

**4.4. Conical Intersection.** The topology of adiabatic electronic potential energy surfaces near a surface crossing has interested researchers for years.<sup>26,60–66</sup> Of particular interest are conical intersections, degenerate points of two adiabatic surfaces that have dimension  $N - 2$  in nuclear space, where  $N$  is the number of internal nuclear coordinates. There has been a great deal of interest into how important conical intersections are to nonadiabatic photoreactions.<sup>60,65</sup> The standard mantra of organic photochemists is that all flexible molecules relax through conical intersections.<sup>67</sup> Thus, for example, one might argue that because compound M has a flexible bridge, the molecule should be able to explore nuclear coordinate space until a conical intersection is reached, and as a result, EET should go through a conical seam.

Indeed, our on-the-fly surface hopping dynamics have allowed us to show definitively that the energy transfer reaction in Closs compound M does proceed through a conical intersection near the transition state. Figure 10 shows that

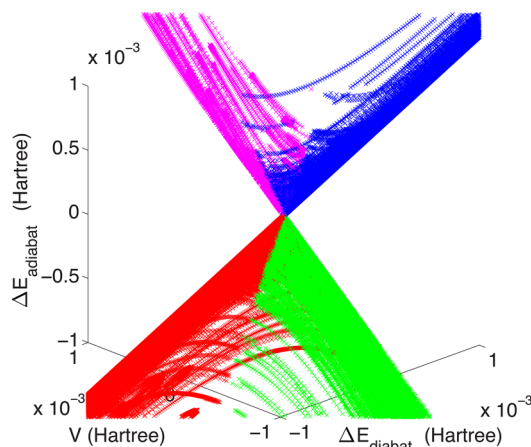


**Figure 10.** Detail of Figure 6 showing the crossing region. The adiabats appear to touch forming a conical intersection. Individual trajectory points show that trajectories typically go very close to the conical intersection in order for the system to transition from the donor diabatic to the acceptor diabatic state. Note that the individual trajectories move on roughly constant  $V$  curves. Colors have the same significance as in Figure 3.

trajectory points come very near to  $(0,0,0)$ , the point representing a conical intersection. As the surfaces rise away from this point in our reaction coordinate system, there is a clear linear behavior for  $\Delta E_{\text{adiabat}}$  as a function of  $\Delta E_{\text{diabat}}$  and  $V$  in accordance with the behavior expected for a conical intersection.

To confirm beyond any doubt that this intersection is indeed conical, Figure 11 provides a plot of the derivative couplings in

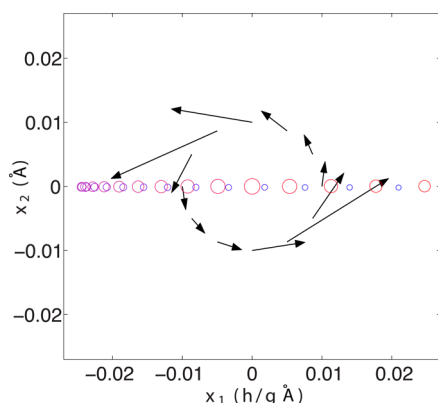


**Figure 11.** Plot of the branching plane showing the relative magnitude of the derivative couplings (black arrows) around our point of closest approach (central largest circle) to the conical intersection. The circles show the path of closest approach to the conical intersection from our dynamical simulation. Each circle represents the projection of the nuclear coordinates at a single time step into the branching plane. The circle radius is inversely proportional to the distance from the branching plane, and the circle color represents increasing time from red to blue. For this trajectory, the molecule enters from the right and passes extremely close to the conical intersection before turning around and exiting back on the right. Note the nonvanishing curl of the derivative coupling corresponds to a nonzero Berry's phase, which proves the existence of a conical intersection. The labels  $x_1$  and  $x_2$  represent rescaled vectors spanning the plane of the adiabatic force difference and the derivative coupling.

the branching plane. The branching plane was determined from the derivative coupling and adiabatic force difference for the nuclear geometry lying closest to the intersection from our trajectories in Figure 10.<sup>68</sup> After the derivative couplings and adiabatic force differences were orthonormalized, we calculated the adiabatic energy difference on a circle of radius 0.01 Å about the trajectory geometry nearest the conical intersection. Next, the coordinates were rescaled to make the conical intersection more circular rather than elliptical; without rescaling, the conical intersection appeared highly eccentric. (In other words, with the convention that the adiabatic energy difference around the conical intersection is  $\propto (g^2 x^2 + h^2 y^2)^{1/2}$ , we found the parameter ratio  $h/g \sim 0.01$ .) Finally, we calculated the derivative couplings around a circle in these rescaled dimensions for Figure 11. Note the nonzero curl of the derivative coupling vector field corresponds to a nonzero Berry's phase; this behavior confirms the existence of a conical intersection.

Let us now describe the nuclear geometries and dynamical motions that are found in the energy transfer event (Figures 12, 13, and 14) going through the conical intersection. Although Figure 10 might seem to suggest that the conical intersection is a single point, the conical intersection is really a  $N - 2$  dimensional surface. As a result, it is possible to observe many different geometries at the conical intersection. In practice, we find that all of our nuclear geometries near the conical intersection seam look similar to the two geometries shown in Figure 12 (which are closely related themselves). The usual geometries on the donor and acceptor sides of the conical intersection are shown in Figure 13. Clearly, torsional motion about the methylene bridge is paramount for the overall electronic relaxation.<sup>69</sup> Given the uniformity of geometries around the conical intersection, our simulations would seemingly confirm the intuitive photochemical model that

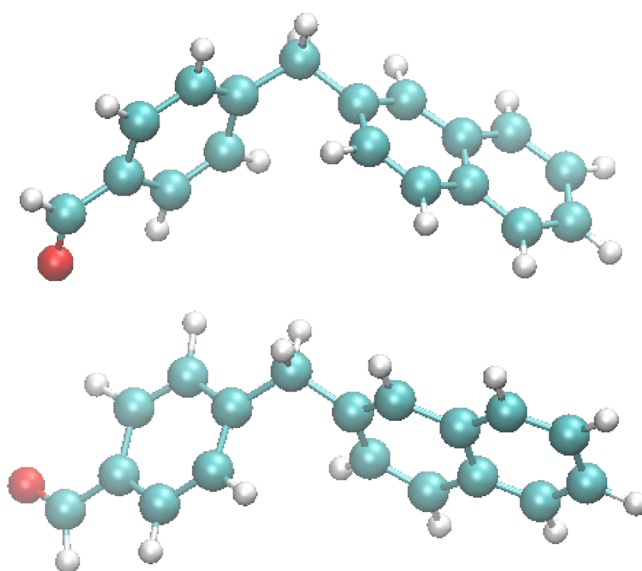


**Figure 12.** Two geometries that are found very close to the conical intersection. They are nearly mirror images.

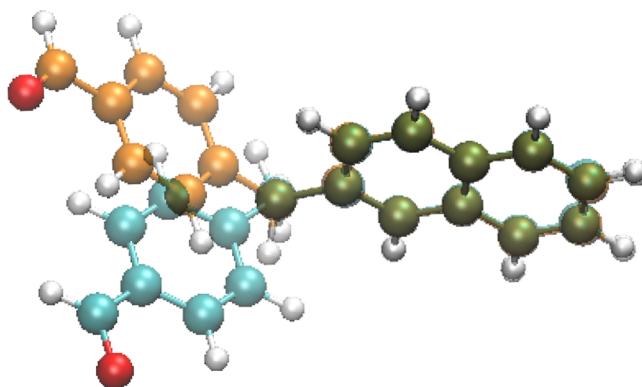


**Figure 13.** Comparison of geometries on the acceptor and donor sides of the conical intersection. Here, the acceptor (orange) and donor (blue) structures are superimposed, one on top of the other. Clearly, the difference between the two geometries is a twist around the methylene bridge so that the donor and acceptor rings are at a different angle relative to one another.

flexible chromophores relax primarily through localized seams of conical intersection at low-lying energies.<sup>67</sup> However, Figure 14 suggests that at the conical intersection itself torsional motion is less important. Figure 14 shows the  $\vec{g} = \vec{\nabla}(\Delta E_{\text{diabat}})$  and  $\vec{h} = \vec{\nabla}V$  directions that break the conical intersection, and the  $\vec{g}$  direction is mostly an in-plane motion. This analysis suggests that there are three stages of important motions in EET for compound M. First, the system must climb the potential energy surface to get to the conical intersection at the crossing point, and torsional motion is the dominant motion for this process. Second, in-plane motion in the carbon rings is the primary nuclear motion guiding the molecule locally through the conical intersection. Finally, additional torsional motion is necessary to relax into the product well. This trajectory description will be expanded on in the next section.

Lastly, a few words are in order about conical intersections and decoherence and the corresponding implications. The decoherence rate for EET through a conical intersection is rapid for two reasons: (i) A conical intersection is a seam of dimension  $N - 2$ , and probabilistically, leaving the vicinity of a

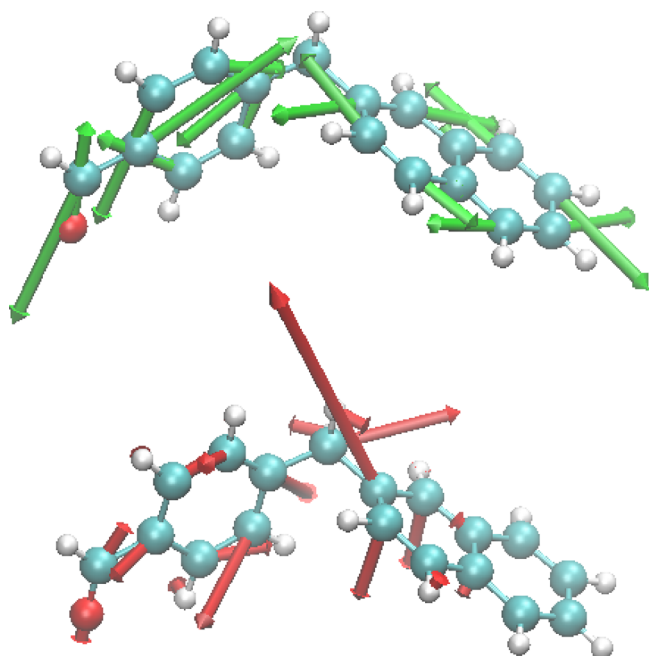


**Figure 14.** Green arrows show the  $\vec{g} = \vec{\nabla}(\Delta E_{\text{diabat}})$  direction (which is also the direction of the derivative coupling), and red arrows show the  $\vec{h} = \vec{\nabla}V$  direction. Note that the magnitude of the  $\vec{g}$  vectors and  $\vec{h}$  vectors have been scaled to make the size of the arrows comparable ( $\vec{h}$  is scaled by a factor of 50 relative to  $\vec{g}$ ).

conical intersection should be almost instantaneous. (ii) The  $T_1/T_2$  adiabatic force differences are extremely different.<sup>70</sup> Together these factors should lead to rapid decoherence.

## 5. DISCUSSION: QUASI-1-DINTERPRETATION

The large difference between  $g$  and  $h$  discussed above suggests that dynamics near the conical intersection might be well approximated by a 1-D model. In particular, because  $h = |\vec{\nabla}V|$  is always small at the crossing point, each trajectory is apparently moving along a single reaction coordinate  $\Delta E_{\text{diabat}}$  at the time of every nonadiabatic event. Indeed, in Figure 15, we show a histogram of the  $g^2$  and  $h^2$  values as sampled at the crossing point ( $E_{\text{diabat}} = 0$ ). Here,  $g = |\vec{\nabla}(\Delta E_{\text{diabat}})|$  and  $h = |\vec{\nabla}V|$ . Notice that  $h^2 \approx 0$ , so that a 1-D model of the dynamics for the Closs system M may be possible. (In agreement, the dynamics in Figures 6, 10, and 11 appear to be 1-D with each trajectory

moving with a roughly constant  $V$ ). This  $h^2 \approx 0$  behavior of the conical intersection has previously been observed in non-adiabatic intramolecular electron transfer.<sup>71</sup>

Before seeking a 1-D transition state explanation of the EET event, we note that if an effective 1-D reaction coordinate does exist, it must be a curved coordinate. This is evident from Figure 13, which shows that the overall reaction coordinate involves a twisting motion around the methylene bridge. At the same time, Figure 14 shows the reaction coordinate locally at the conical intersection. At the conical intersection, the reaction coordinate (represented mostly by  $\vec{g} = \vec{\nabla}(\Delta E_{\text{diabat}})$  since  $|\vec{g}| \gg |\vec{h}|$ ) involves an in-plane ring distortion. Both the overall nuclear relaxation and the local driving force at the crossing point must be addressed by any transition state theory calculation, and as such, a 1-D reaction coordinate must be very curved.

We are now prepared to make a transition state theory estimate of the EET rate from compound M. We focus first on velocities. In Figure 16, we show histograms of the velocities in the direction of the gradient of the diabatic energy difference,  $\vec{g} = \vec{\nabla}(\Delta E_{\text{diabat}})$ , and the direction of the gradient of the diabatic coupling,  $\vec{h} = \vec{\nabla}V$ , as sampled at the crossing point ( $E_{\text{diabat}} = 0$ ). The total histogram of velocities in the  $\vec{g}$  direction (Figure 16a) shows an interesting (non-Gaussian) bimodality. After analyzing trajectories, one finds that the bimodal behavior arises because, in the case of both forward and backward moving trajectories, the velocity distribution is not peaked at zero. Indeed, Figure 16b and c show the velocity distributions for the cases of first and second crossings, where one finds that positive velocities correspond to trajectories moving toward the crossing from the donor well (first crossing), and the negative velocities correspond to trajectories that have hopped into the upper cone and are now returning to the crossing moving back toward the donor well (second crossing). Note that neither the velocity distribution in Figure 16b nor the distribution in Figure 16c is peaked around zero.

Both the forward and the backward crossings are important in our simulations, so that Gaussian behaviors should not be expected when we sample only over trajectories that start in the reactant basin. Note though that the average kinetic energy is roughly  $(1/2)kT$  for motion in the  $\vec{g}$  direction so the velocity distribution in Figure 16a is not just the result of a low barrier crossing.

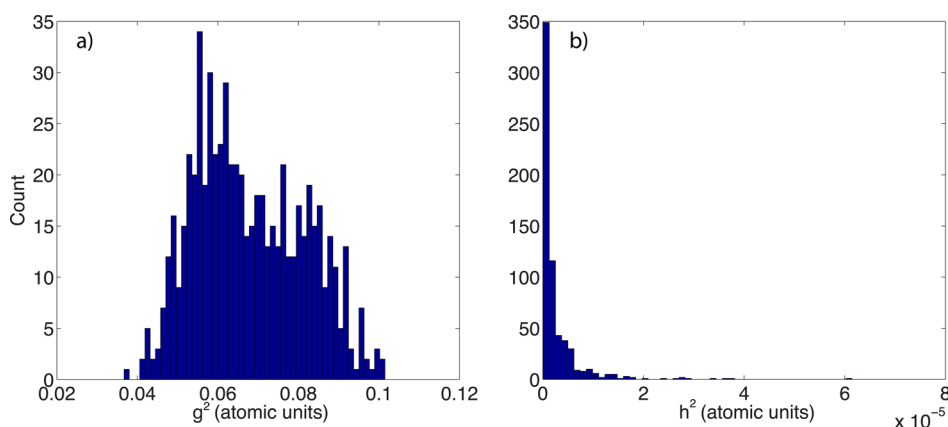


**Figure 15.** (a) Histogram of  $g^2$  for the conical intersection at the crossing point ( $E_{\text{diabat}} = 0$ ) for all the trajectories ( $g = |\vec{\nabla}(\Delta E_{\text{diabat}})|$ ). (b) Histogram of  $h^2$  for the conical intersection at the crossing point ( $E_{\text{diabat}} = 0$ ) for all the trajectories ( $h = |\vec{\nabla}V|$ ).



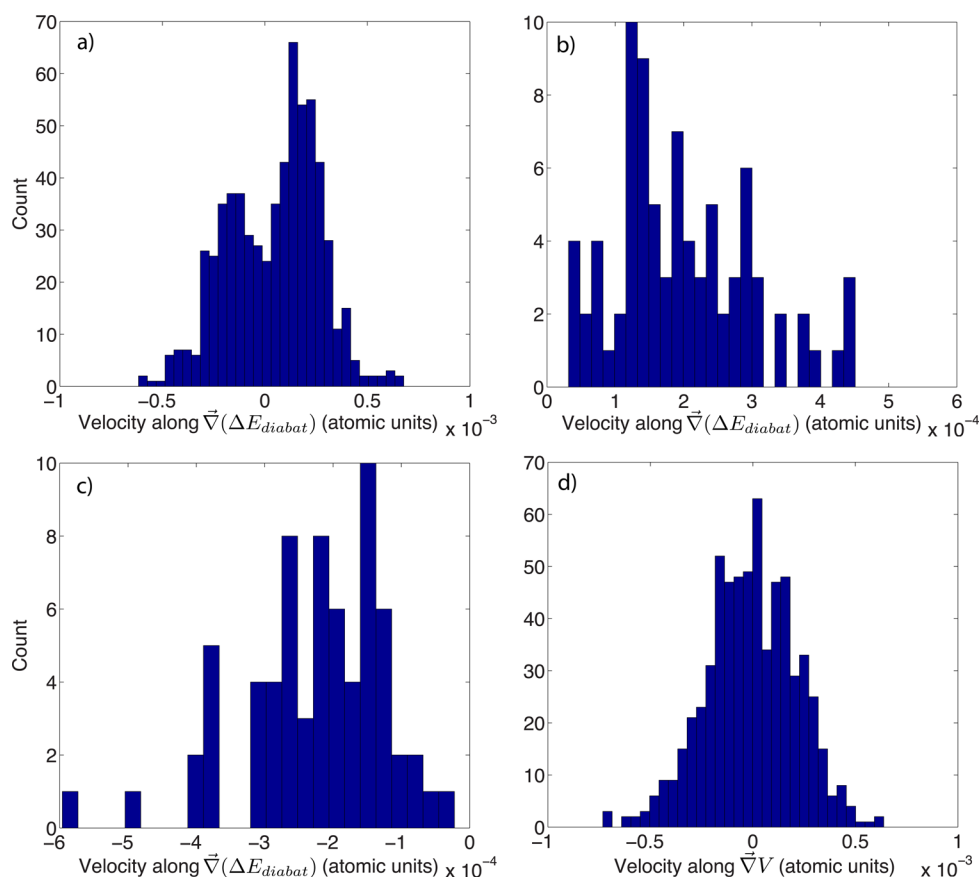


**Figure 16.** Histograms of the velocity components at the crossing ( $E_{\text{diabat}} = 0$ ) measured along different directions: (a)  $\vec{V}(\Delta E_{\text{diabat}})$  for all crossings, (b)  $\vec{V}(\Delta E_{\text{diabat}})$  for the first crossing only, (c)  $\vec{V}(\Delta E_{\text{diabat}})$  for the second crossing only, and (d)  $\vec{V}V$  for all crossings.

Continuing the analysis of trajectories during their first and second crossings, we find that all trajectories that cross twice have hopped at least once; in other words, all trajectories that cross while staying on the lower adiabatic relax directly onto the acceptor. As such, it might be reasonable to apply nonadiabatic transition state theory where we assume that the state-crossings happen at or near the transition state barrier in the ground state (i.e., Marcus theory).

To apply Marcus theory, Figure 17 shows a histogram of the square of the diabatic coupling as sampled from the seam of crossing points ( $E_{\text{diabat}} = 0$ ). The histogram is peaked at zero, implying that the trajectories are most likely to cross right near

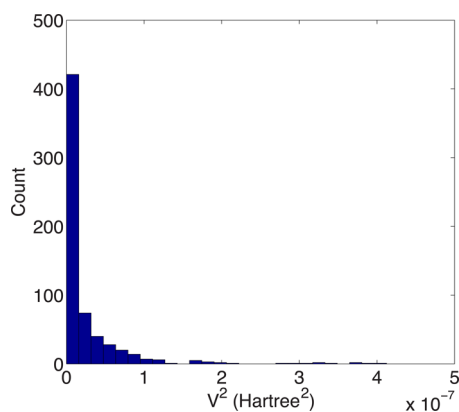


**Figure 17.** Histogram of the square of the diabatic coupling at the crossing ( $E_{\text{diabat}} = 0$ ).

the conical intersection. The square root of the average value of the squares of the diabatic couplings in Figure 17 is  $(\langle V^2 \rangle)^{1/2} = 1.85 \times 10^{-4}$  Hartree. All the reorganization energies for this system are given in Table 1. Using these reorganization energies and couplings, we can calculate EET rates also given in Table 1.

**Table 1. Reorganization Energies and Transition Rates<sup>a</sup>**

basis	$E_r$ (Hartree)	$\epsilon_0$ (Hartree)	$1/k$ (ps)
3-21G	0.0489	-0.0140	1910
	0.0369	-0.0140	99.4
6-31G**	0.0308	-0.0209	4.98
	0.0325	-0.0209	6.59

<sup>a</sup>Note the two reorganization energies are from the two diabatic wells:  $E_r = E(T_2, D^*A) - E(T_1, DA^*)$  and  $E_r = E(T_2, DA^*) - E(T_1, D^*A)$ . (These energies are different because the wells are not harmonic.) The driving force is given by  $\epsilon_0 = E(T_1, DA^*) - E(T_1, D^*A)$ . The Marcus rates are given by  $k = (2\pi|V|^2)/(\hbar(4\pi E_r kT)^{1/2}) \exp(-(E_r + \epsilon_0)^2/(4E_r kT))$ . Here,  $kT$  is the temperature. The experimental value for  $1/k$  is 20 ps.<sup>1</sup>

From Table 1, we find that the Marcus theory does yield a reasonably accurate EET rate by using a combination of dynamically averaged diabatic coupling in a 3-21G basis and reorganization energies in the 6-31G\*\* basis. Admittedly, this finding should probably be taken with a grain of salt. After all, Marcus theory assumes a constant diabatic coupling (not an average over crossing geometries) and harmonic potential energy surfaces (whereas we find two different reorganization

energies). A more rigorous approach would be to calculate the EET rate through the conical intersection with the perturbative formalism of Izamaylov et al.<sup>72,73</sup> At the same time, one might not be surprised that using better potential energy surfaces yields a better final rate. In the end, our intuition is that relaxation in compound M likely can be explained quite well from a quasi-1-D theory with the  $\vec{g}$  direction as the effective reaction coordinate. That being said, we cannot prove as much right now. Our understanding of EET for compound M would benefit by balancing our current dynamics calculations in a small basis with future high accuracy potential energy surfaces from a large basis (computed at a suitably high level of theory).

## 6. CONCLUSIONS

We have modeled the dynamics of energy transfer in compound M using surface hopping and electronic structure computed on the fly. Our methods yield excellent results for the transfer rate when compared with the experimental value, although this may be fortuitous given our small basis set. Most importantly, our dynamical investigation has allowed us to explore the nature of the reaction in detail. We found the energy transfer mechanism to occur via a conical intersection, and we explored the geometries in the vicinity of the conical intersection. Both (i) bending and twisting of the methylene bridge and (ii) in-plane ring distortion are essential for achieving efficient EET. In particular, our analysis of the important motions in EET for compound M revealed that torsional motions are important to reach the conical intersection but that in-plane motions in the rings are dominant as the molecule passes through the conical intersection itself. Finally, we were able to estimate the coherence time of the energy transfer process to be  $\sim 20$  fs.

Altogether, this work confirms the prevalent intuition that for floppy (rather than rigid) molecules, EET proceeds through conical intersections. However, we note that for compound M the conical intersection is highly elliptical and quasi-one-dimensional rate theories might be possible. This remains to be seen. Future work involving applications of surface hopping to both ET and EET for real molecular systems is ongoing.

## AUTHOR INFORMATION

### Corresponding Author

\*E-mail: landrybr@gmail.com.

### Notes

The authors declare no competing financial interest.

## ACKNOWLEDGMENTS

We thank Shervin Fatehi, Ethan Alguire, Qi Ou, and Sharon Hammes-Schiffer for helpful theory discussions during the course of this work. We acknowledge very helpful experimental discussions with Mike Fayer and Piotr Piotrowiak. We thank the DoD High Performance Computing Modernization Program for computer time. This work was supported by the Air Force Office of Science Research PECASE award under AFOSR Grant FA9550-13-1-0157.

## REFERENCES

- (1) Closs, G. L.; Piotrowiak, P.; MacInnis, J. M.; Fleming, G. R. *J. Am. Chem. Soc.* **1988**, *110*, 2652–2653.
- (2) Closs, G. L.; Johnson, M.; Miller, J. R.; Piotrowiak, P. *J. Am. Chem. Soc.* **1989**, *111*, 3751–3753.
- (3) Marcus, R. A. *J. Chem. Phys.* **1956**, *24*, 966–978.
- (4) Place, I.; Farran, A.; Deshayes, K.; Piotrowiak, P. *J. Am. Chem. Soc.* **1998**, *120*, 12626–12633.
- (5) Subotnik, J. E.; Vura-Weis, J.; Sodt, A. J.; Ratner, M. A. *J. Phys. Chem. A* **2010**, *114*, 8665–8675.
- (6) Cave, R. J.; Newton, M. D. *Chem. Phys. Lett.* **1996**, *249*, 15–19.
- (7) Voityuk, A. A.; Rosch, N. J. *Chem. Phys.* **2002**, *117*, S607–S616.
- (8) Hsu, C.-P.; You, Z.-Q.; Chen, H.-C. *J. Phys. Chem. C* **2008**, *112*, 1204–1212.
- (9) Chen, H.-C.; You, Z.-Q.; Hsu, C.-P. *J. Chem. Phys.* **2008**, *129*, 084708.
- (10) Hsu, C.-P. *Acc. Chem. Res.* **2009**, *42*, 509–518.
- (11) Subotnik, J. E.; Yaganeh, S.; Cave, R. J.; Ratner, M. A. *J. Chem. Phys.* **2008**, *129*, 244101.
- (12) Subotnik, J. E.; Cave, R. J.; Steele, R. P.; Shenvi, N. *J. Chem. Phys.* **2009**, *130*, 234102.
- (13) Kuharski, R. A.; Bader, J. S.; Chandler, D.; Sprik, M.; Klein, M. L.; Impey, R. W. *J. Chem. Phys.* **1988**, *89*, 3248.
- (14) Nitzan, R. A. *Chemical Dynamics in Condensed Phases: Relaxation, Transfer, and Reactions in Condensed Molecular Systems*; Oxford University Press: Oxford, U.K., 2006.
- (15) Medvedev, E. S.; Stuchebrukhov, A. A. *J. Chem. Phys.* **1997**, *107*, 3821–3831.
- (16) Jang, S.; Newton, M. D. *J. Chem. Phys.* **2005**, *122*, 024501.
- (17) Note that we have substituted a 4-benzaldhydryl donor for the 4-benzophenonyl donor that Closs and co-workers originally studied.<sup>1</sup> We made this substitution for the increased ease in the electronic structure calculations for the 4-benzaldhydryl system. This substitution is not expected to effect the energy transfer rate.
- (18) Tully, J. C. *J. Chem. Phys.* **1990**, *93*, 1061–1071.
- (19) Landry, B. R.; Subotnik, J. E. *J. Chem. Phys.* **2012**, *137*, 22A513.
- (20) Shim, S.; Rebentrost, P.; Valleeau, S.; Aspuru-Guzik, A. *Biophys. J.* **2012**, *102*, 649–660.
- (21) Nassimi, A.; Bonella, S.; Kapral, R. *J. Chem. Phys.* **2010**, *133*, 134115.
- (22) Kim, H. W.; Kelley, A.; Park, J. W.; Rhee, Y. M. *J. Am. Chem. Soc.* **2012**, *134*, 11640–11651.
- (23) Lobaugh, J.; Rossky, P. J. *J. Phys. Chem. A* **1999**, *103*, 9432–9447.
- (24) Fernandez-Alberti, S.; Kleiman, V. D.; Tretiak, S.; Roitberg, A. E. *J. Phys. Chem. A* **2009**, *113*, 7535–7542.
- (25) Nelson, T.; Fernandez-Alberti, S.; Roitberg, A. E.; Tretiak, S. *J. Chem. Phys.* **2013**, *138*, 224111.
- (26) Toniolo, A.; Olsen, S.; Manohar, L.; Martinez, T. J. *Farad. Discuss.* **2004**, *127*, 149–163.
- (27) Nachtigallova, D.; Aquino, A. J. A.; Szymczak, J. J.; Barbatti, M.; Hobza, P.; Lischka, H. *J. Phys. Chem. A* **2011**, *115*, S247–S255.
- (28) Tapavicza, E.; Bellchambers, G. D.; Vincent, J. C.; Furche, F. *Phys. Chem. Chem. Phys.* **2013**, *15*, 18336–18348.
- (29) Shao, Y.; Fusti-Molnar, L.; Jung, Y.; Kussmann, J.; Ochsenfeld, C.; Brown, S. T.; Gilbert, A. T. B.; Slipchenko, L. V.; Levchenko, S. V.; O'Neill, D. P.; DiStasio, R. A., Jr.; Lochan, R. C.; Wang, T.; Beran, G. J. O.; Besley, N. A.; Herbert, J. M.; Lin, C. Y.; Van Voorhis, T.; Chien, S. H.; Sodt, A.; Steele, R. P.; Rassolov, V. A.; Maslen, P. E.; Korambath, P. P.; Adamson, R. D.; Austin, B.; Baker, J.; Byrd, E. F. C.; Daschel, H.; Doerksen, R. J.; Dreuw, A.; Dunietz, B. D.; Dutoi, A. D.; Furlani, T. R.; Gwaltney, S. R.; Heyden, A.; Hirata, S.; Hsu, C.-P.; Kedziora, G.; Khaliullin, R. Z.; Klunzinger, P.; Lee, A. M.; Lee, M. S.; Liang, W. Z.; Lotan, I.; Nair, N.; Peters, B.; Proynov, E. I.; Pieniazek, P. A.; Rhee, Y. M.; Ritchie, J.; Rosta, E.; Sherrill, C. D.; Simmonett, A. C.; Subotnik, J. E.; Woodcock, L. W., III; Zhang, W.; Bell, A. T.; Chakraborty, A. K.; Chipman, D. M.; Keil, F. J.; Warshel, A.; Hehre, W. J.; Schaefer, H. F., III; Kong, J.; Krylov, A. I.; Gill, P. M. W.; Head-Gordon, M. *Phys. Chem. Chem. Phys.* **2006**, *8*, 3172–3191.
- (30) Fatehi, S.; Subotnik, J. E. *J. Phys. Chem. Lett.* **2012**, *3*, 2039–2043.
- (31) To do this we calculated  $\sum_{\alpha} |\dot{\vec{R}}^{\alpha} \cdot \vec{d}_{12}^{\alpha}|$ , where the  $\alpha$  index is over the nuclear dimension,  $\vec{R}$  is the nuclear velocity, and  $\vec{d}_{12}$  is the derivative coupling. If the sum was less than a tolerance (0.05), then

the larger time step could be used; otherwise, the shorter time step was used.

(32) Fernandez-Alberti, S.; Roitberg, A. E.; Nelson, T.; Tretiak, S. *J. Chem. Phys.* **2012**, *137*, 014512.

(33) Fatehi, S.; Alguire, E.; Subotnik, J. E. *J. Chem. Phys.* **2013**, *139*, 124112.

(34) Yarkony, D. R. *J. Phys. Chem. A* **1998**, *102*, 8073–8077.

(35) Landry, B. R.; Falk, M. J.; Subotnik, J. E. *J. Chem. Phys.* **2013**, *139*, 211101.

(36) However, the diabatic couplings were large enough that A-FSSH and FSSH gave similar results as discussed in Section 4.1.

(37) Webster, F.; Rossky, P. J.; Friesner, R. A. *Comput. Phys. Commun.* **1991**, *63*, 494–522.

(38) Webster, F.; Wang, E. T.; Rossky, P. J.; Friesner, R. A. *J. Chem. Phys.* **1994**, *100*, 4835–4847.

(39) Schwartz, B. J.; Bittner, E. R.; Prezhdo, O. V.; Rossky, P. J. *J. Chem. Phys.* **1996**, *104*, 5942–5955.

(40) Wong, K. F.; Rossky, P. J. *J. Chem. Phys.* **2002**, *116*, 8418–8428.

(41) Wong, K. F.; Rossky, P. J. *J. Chem. Phys.* **2002**, *116*, 8429–8438.

(42) Prezhdo, O. V.; Rossky, P. J. *J. Chem. Phys.* **1997**, *107*, 825–834.

(43) Prezhdo, O. V. *J. Chem. Phys.* **1999**, *111*, 8366–8377.

(44) Bedard-Hearn, M. J.; Larsen, R. E.; Schwartz, B. J. *J. Chem. Phys.* **2005**, *123*, 234106.

(45) Larsen, R. E.; Bedard-Hearn, M. J.; Schwartz, B. J. *J. Phys. Chem. B* **2006**, *110*, 20055–20066.

(46) Zhu, C.; Jasper, A. W.; Truhlar, D. G. *J. Chem. Phys.* **2004**, *120*, 5543–5557.

(47) Zhu, C.; Nangia, S.; Jasper, A. W.; Truhlar, D. G. *J. Chem. Phys.* **2004**, *121*, 7658–7670.

(48) Jasper, A. W.; Truhlar, D. G. *J. Chem. Phys.* **2005**, *123*, 064103.

(49) Zhu, C.; Jasper, A. W.; Truhlar, D. G. *J. Chem. Theory Comput.* **2005**, *1*, 527–540.

(50) Jasper, A. W.; Truhlar, D. G. *J. Chem. Phys.* **2007**, *127*, 194306.

(51) Fang, J. Y.; Hammes-Schiffer, S. *J. Chem. Phys.* **1999**, *110*, 11166–11175.

(52) Subotnik, J. E.; Shenvi, N. *J. Chem. Phys.* **2011**, *134*, 024105.

(53) Shenvi, N.; Subotnik, J. E.; Yang, W. *J. Chem. Phys.* **2011**, *134*, 144102.

(54) The triplet energy transfer rates in ref 1 were computed by fitting the exponential tail of the decay of the donor absorption and/or the rise of the acceptor absorption. If we assume  $k_{\text{ISC}}^{-1} \approx 10$  ps,<sup>74</sup> then a decent fit of the exponential data should produce accuracy down to about 2 ps in the rate.

(55) Landry, B. R.; Subotnik, J. E. *J. Chem. Phys.* **2011**, *135*, 191102.

(56) The relevant quantity is the Landau–Zener parameter  $\alpha_{\text{LZ}} = (2\pi)/(\hbar|\vec{R} \cdot \Delta\vec{F}|)$ , where  $\vec{R}$  is the nuclear velocity, and  $\Delta\vec{F}$  is the force difference between the two surfaces at the crossing region.  $\alpha_{\text{LZ}} \ll 1$  corresponds to the nonadiabatic regime. Refs 19 and 55 show that for the spin-boson model, FSSH and A-FSSH give very different results in this regime, but the two methods give comparable results when  $\alpha_{\text{LZ}} \sim 1$ .

(57) Hayes, D.; Griffin, G. B.; Engel, G. S. *Science* **2013**, *430*, 1431–1434.

(58) Collini, E.; Wong, C. Y.; Wilk, E. K.; Curmi, P. M. G.; Brumer, P.; Scholes, G. D. *Nature* **2010**, *463*, 644–647.

(59) This procedure may slightly bias our decoherence rate because not all trajectories passing through a crossing region will attempt a hop. We thank Sharon Hammes-Schiffer for raising this point.

(60) Robb, M. A.; Bernardi, F.; Olivucci, M. *Pure Appl. Chem.* **1995**, *67*, 783–789.

(61) Yarkony, D. R. *Rev. Mod. Phys.* **1996**, *68*, 985–1013.

(62) Yarkony, D. R. *Acc. Chem. Res.* **1998**, *31*, 511–518.

(63) Yarkony, D. R. *J. Phys. Chem. A* **1998**, *102*, 8073–8077.

(64) Yarkony, D. R. *J. Chem. Phys.* **1999**, *110*, 701–705.

(65) Yarkony, D. R. *J. Phys. Chem. A* **2001**, *105*, 6277–6293.

(66) Levine, B. G.; Martinez, T. J. *Annu. Rev. Phys. Chem.* **2007**, *58*, 613–634.

(67) Turro, N. J.; Ramamurthy, V.; Scaiano, J. C. *Principles of Molecular Photochemistry: An Introduction*; University Science Books: Herndon, VA, 2009.

(68) The branching plane can also be determined using the derivatives of BoysOV localized diabatic energies and couplings.<sup>33,75</sup>

(69) Kim, H.; Hwang, H.; Rossky, P. J. *J. Phys. Chem. A* **2006**, *110*, 11223–11229.

(70) All evidence suggests that the decoherence rate should be proportional to the difference in the forces between the two surfaces.<sup>19,39</sup>

(71) Fernandez, E.; Blancafort, L.; Olivucci, M.; Robb, M. A. *J. Am. Chem. Soc.* **2000**, *122*, 7528–7533.

(72) Izmaylov, A. F.; Mendive-Tapia, D.; Bearpark, M. J.; Robb, M. A.; Tully, J. C.; Frisch, M. J. *J. Chem. Phys.* **2011**, *135*, 234106.

(73) Endicott, J. S.; Joubert-Doriol, L.; Izmaylov, A. F. *J. Chem. Phys.* **2014**, *141*, 034104.

(74) Tamai, N.; Asahi, T.; Masuhara, H. *Chem. Phys. Lett.* **1992**, *198*, 413–418.

(75) Alguire, E. C.; Fatehi, S.; Shao, Y.; Subotnik, J. E. *J. Phys. Chem. A* **2014**, DOI: 10.1021/jp411107k.